Process Safety and Environmental Protection 174 (2023) 891–900

Contents lists available at ScienceDirect

Process Safety and Environmental Protection

journal homepage: www.journals.elsevier.com/process-safety-and-environmental-protection

Fabrication of graphene nanoplatelets/MgAl-layered double hydroxide nanocomposites as efficient support for gold nanoparticles and their catalytic performance in 4-nitrophenol reduction

Meriem Banou [a,d], Yubiao Niu [b,c], Fatima Ammari [d,*], Tom Dunlop [c], Richard E. Palmer [b], Chedly Tizaoui [a,*]

[a] Water and Resources Recovery Research Lab, Department of Chemical Engineering, Faculty of Science and Engineering, Swansea University, Swansea, UK
[b] Nanomaterials Lab, Mechanical Engineering, Faculty of Science and Engineering, Swansea University, Swansea, UK
[c] The Advanced Imaging of Materials (AIM) Facility, Faculty of Science and Engineering, Swansea University, Swansea, UK
[d] LGPC, Department of Chemical Process Engineering, Ferhat-Abbas Sétif-1 University, Setif, Algeria

ARTICLE INFO

Keywords:
Hydrotalcite
Gold nanoparticles
Graphene
Nitrophenol
Reduction

ABSTRACT

The catalytic reduction of 4-nitrophenol is of considerable importance to a multitude of applications and industries. The present work introduces a new catalyst (AuNP/GNP/MgAl-LDH) containing gold nanoparticles (AuNP) supported on graphene nanoplatelets (GNP) intercalated in Mg Al layered double hydroxides (MgAl-LDH) for the reduction of 4-nitrophenol to 4-aminophenol using $NaBH_4$ as a reducing agent. The catalyst was characterised by FTIR, XRD, STEM, TEM, and BET specific surface area. The XRD analysis showed the presence of crystalline phases of gold on the supports, while TEM demonstrated that MgAl-LDH provided uniform binding sites for AuNPs and prevented agglomeration. Similar reaction rate constant was determined for the disappearance of 4-nitrophenol and for the appearance of 4-aminophenol. The reaction rate constant was the highest for AuNP/GNP/MgAl-LDH, followed by AuNP/MgAl-LDH and AuNP/GNP. AuNP/GNP/MgAl-LDH was found stable after five repeated cycles.

1. Introduction

The catalytic reduction of 4-nitrophenol (4-NP) is a widely used reaction to evaluate the activity of catalysts. Strachan et al. (2020) attributed the ubiquitous use of the 4-NP reaction to three elements, including: the reaction does not proceed in the absence of a catalyst, the reaction can be conducted in aqueous solutions at ambient conditions, and the monitoring of the reaction can be done using simple and readily available instruments (i.e. UV/Vis spectrophotometers). This reaction has also importance in the context of environmental protection and chemical manufacturing. This is because, nitroaromatics are widely used for the manufacture of a variety of chemicals (e.g. dyestuffs, pharmaceutical products, agricultural chemicals, and polymers) and as a result they are widely distributed in the environment (Gemini et al., 2005). Amongst nitroaromatics, 4-nitrophenol is probably the most important due to its large quantity use and potential impact on the environment. If unproperly discharged into the environment, 4-nitrophenol has potential to cause environmental and human health negative effects (Gemini et al., 2005). The reduction reaction of 4-nitrophenol is also a useful reaction in the context of chemical manufacturing; for example, the reduction of 4-nitrophenol to 4-aminophenol is an essential reaction to produce analgesic and antipyretic drugs. Therefore, the catalytic reduction of 4-nitrophenol reaction is of considerable importance to a multitude of applications and industries.

The reduction reaction of 4-NP is typically conducted in aqueous solutions in the presence of sodium borohydride ($NaBH_4$) and a metal catalyst. The borohydride is commonly used in molar excess to 4-NP and the product that results from the reaction is 4-aminophenol (4-AP). Although the reaction is thermodynamically possible, the repelling nature of the reactants, because they ionise in solution to negatively charged ions (i.e. $(NO_2)C_6H_4O^-$ and BH_4^-), limits the kinetics of the reaction. The metal catalyst is thus essential to overcome the kinetic barrier by adsorbing the reactants, which facilitates electron transfer and progresses the redox reaction.

Many metal-supported catalysts have been studied for the reduction reaction of 4-NP to 4-AP including *Au, Ti, Pd, Cu, Co, Mo, Ni Fe, Ag, Zn, Pt*

* Corresponding authors.
E-mail addresses: ammarifatima@yahoo.fr (F. Ammari), c.tizaoui@swansea.ac.uk (C. Tizaoui).

https://doi.org/10.1016/j.psep.2023.04.051
Received 27 September 2022; Received in revised form 29 January 2023; Accepted 28 April 2023
Available online 3 May 2023
0957-5820/© 2023 The Author(s). Published by Elsevier Ltd on behalf of Institution of Chemical Engineers. This is an open access article under the CC BY license (http://creativecommons.org/licenses/by/4.0/).

(Alshammari et al., 2020; Hao et al., 2020; Hashimi et al., 2019; Iben Ayad et al., 2020; Verma et al., 2015). Due to their high catalytic activity, gold nanoparticles (AuNPs) are the most used catalysts amongst the studied catalysts (Li and Chen, 2013; Ma et al., 2017). However, there are still obstacles in the use of AuNPs because AuNPs often experience irreversible aggregation during preparation (Chegel et al., 2012), which leads to a loss of the nanoscale size and associated intrinsic surface properties. To resolve this issue, the gold nanoparticles are commonly impregnated on supports using a range of natural and synthetic materials such as zeolites (Kuge and Calzaferri, 2003) metal oxides (Yuzawa et al., 2012), activated carbon (Jordi et al., 1991), carbon nanotubes (CNT) (Zhang et al., 2016), polymers (Bleach et al., 2014), and clays (Zhu et al., 2009). However, in recent years, graphene became the most used support material for AuNPs (Chen et al., 2019; Marinoiu et al., 2020; Plant et al., 2014) due to its favourable electronic structure, high surface area, and high adsorption capacity (Alawi et al., 2019; Beltrán et al., 2019; Cataldi et al., 2018; Novoselov et al., 2005; Novoselov et al., 2004). Graphene is also easy to modulate and functionalise to produce tailored catalysts for specific catalytic applications with or without metal loading (Yam et al., 2020). In contrast, a lesser-known support material is the layered double hydroxide (LDH), which is a 2D inorganic nanostructured basic material commonly known as hydrotalcite. The general formula of an LDH is $[M^{II}_{1-x}M^{III}_{x}(OH)_2]^{x+}$. $[A^{n-}_{x/n}.mH_2O]^{x-}$, where M^{II} is a divalent cation, M^{III} is a trivalent cation, and A^{n-} is an anion. Their crystal structure is based on brucite-like sheets $Mg(OH)_2$ (Richardson, 2013), where part of the M^{II} cations are replaced with M^{III} cations, this replacement generates positively charged [M(^{II})/M(^{III})/OH] layers, which are compensated by anions such as CO_3^{2-}, Cl^-, NO_3^-, or organic anions (Asiabi et al., 2017; Cavani et al., 1991). The presence of generated positive charge is responsible for attracting negatively charged reactants, thus lowering the kinetic barrier, and catalysing chemical reactions.

Although both graphene and LDH materials have separately shown great role in supporting AuNPs and preserving the nanoparticle properties while giving interesting results in many catalytic reactions, their use in a composite form is scarce. Thus, it appeared of great interest to investigate the catalytic behaviour of gold nanoparticle catalysts supported on supports containing both positively charged layers of LDH, to attract reactants, and graphene, to stabilise the gold nanoparticles and enhance charge transfer. This combination of graphene and LDH is novel and is fundamentally plausible to provide favourable conditions for high catalytic reduction of 4-NP. Herein, we report the use of a nanocomposite of graphene nanoplatelets (GNP) and MgAl-LDH as a support material for AuNPs. These materials were characterised using different techniques including Fourier transform infrared spectroscopy (FTIR), X-ray diffraction (XRD), Scanning Transmission Electron Microscopy (STEM), Transmission Electron Microscopy (TEM), and BET specific surface area, and tested for the reduction of 4-NP in aqueous media.

2. Materials and methods

2.1. Materials

Graphene nanoplatelets (GNP) pre-treated by plasma oxygen were purchased from HPlas™ and used as intercalating material for the synthesis of the AuNP/GNP/MgAl-LDH nanocomposite. The lateral average size and thickness of the GNPs were in the range of 0.3–5 μm and < 50 nm, respectively. $MgSO_4$ anhydrous (99 %), $Al_2(SO_4)_3{\cdot}16\ H_2O$ (98 %), $HAuCl_4 3\ H_2O$, NaOH, $NaHCO_3$, and ammonia solution (32 %) were all purchased from Fischer Scientific, UK.

2.2. Preparation of GNP/MgAl-LDH nanocomposite

A colloidal dispersion of GNP was obtained by dispersing 300 mg of GNP in an aqueous solution containing (1 M) NaOH and (0.4 M) $NaHCO_3$. Subsequently, a salt solution of (0.5 M) $MgSO_4$ and (0.15 M) $Al_2(SO_4)_3{\cdot}16\ H_2O$ was added. The resulting black suspension was aged at 333 K for 18 h under stirring (300 rpm). The sample was then filtered, washed, and dried for 12 h at 393 K.

2.3. Preparation of supported gold nanoparticles

The 2 %Au-supported catalysts were prepared by the deposition-precipitation (DP) method described by Haruta et al. (1989). A suitable amount of $HAuCl_4.3\ H_2O$ was dissolved in 120 mL deionised water, then a solution of NH_3 was added to maintain the pH at about 10 before addition of GNP or GNP/MgAl-LDH support. The obtained solution was stirred for 6 h then refluxed for 1 h at 373 K. The resulting solid was filtered, washed thoroughly with deionized water, and dried at 473 K for 4 h.

2.4. Catalyst characterisation

The FT-IR spectral measurements were done using Perkin-Elmer Spectrum 2 with $LiTiO_2$ detector and an optical KBr window enabling data collection in the range 8300–400 cm^{-1}. The diffraction experiments were carried out on a D8 Discover (Bruker) A Cu Kα1 X-ray radiation source run at 40 kV and 40 mA. The diffraction patterns were recorded from 0° to 80° of 2θ with a step size of 0.04°.

Transmission Electron Microscopy (TEM) and Scanning Transmission Electron Microscopy (STEM) imaging of the materials were performed using a Thermo Scientific Talos F200X Transmission Electron Microscope operating at 200 kV under high-angle annular dark-field (HAADF) mode. Samples were prepared by dispersing the catalyst powder in high purity ethanol using ultra-sonication then 50 μL of the suspension was dropped onto holey carbon coated copper grids followed by evaporation of the solvent. The Java program for Image processing and analysis (ImageJ) software was used to calculate the diameter of particles and count the particles in the resulted images. The mean particle size was calculated by the Sauter mean diameter Eq. (1).

$$D[3,2] = \frac{\sum_{1}^{N} D_i^3 n_i}{\sum_{1}^{N} D_i^2 n_i} \quad (1)$$

where: D_i is the diameter of the i^{th} particle and n_i is the number of particles that have the same diameter D_i.

The specific surface area, pore volume, and pore size distributions of the catalysts were determined by the Brunauer–Emmett–Teller (BET) and Barrett–Joyner–Hallender (BJH) models using N_2 adsorption/desorption isotherms conducted at 77 K (Nova 200e, Quantachrome Instruments). The samples were degassed at 120 °C for 6 h before nitrogen adsorption/desorption measurements were done. Quantachrome NovaWin package was used for data acquisition and analysis.

2.5. Reduction of 4-nitrophenol

The reduction of 4-nitrophenol was carried out in aqueous liquid solutions at ambient temperature. A 10 mg of the catalyst, previously dispersed in 10 mL of distilled water, was added to 10 mL of freshly prepared aqueous solution of $NaBH_4$ (10 mmol) and the obtained mixture was then added to a 10 mL of 4-NP solution (0.3 mmol) under vigorous stirring (the total volume of the solution was 30 mL). The reaction progress was monitored by UV-Vis spectrophotometry (Lambda 35, PerkinElmer) in the wavelength range of 200–600 nm using 1 mL samples of the reaction solution withdrawn at regular times then filtered and analysed. In a typical UV-Vis spectra (e.g. Fig. 5A), the light absorption at 400 nm corresponds to 4-NP with $NaBH_4$ in solution, whereas the absorption at 298 nm corresponds to 4-aminophenol (4-AP), the reaction product. Since $NaBH_4$ was used in excess in the reduction reaction, the catalytic reduction of 4-NP was evaluated

according to the pseudo-first-order kinetic model (Qiu et al., 2012), which can be expressed by Eq. (2), considering the disappearance of 4-NP, or by Eq. 3, considering the formation of 4-AP. Based on the Beer-Lambert Law, the concentrations of 4-NP and 4-AP are linked to light absorbances measured at 400 nm (Abs_{400}) and 298 nm (Abs_{298}) by $Abs_{400}/(\varepsilon_{NP}.L)$ and $Abs_{298}/(\varepsilon_{AP}.L)$, respectively; where ε_{NP} and ε_{AP} are the molar extinction coefficients of 4-NP and 4-AP at 400 nm and 298 nm respectively, and L is the pathlength of the UV–vis cuvette (1 cm).

In the reaction solution, the absorbance measured at 400 nm is due to 4-NP and is not significantly affected by interference from 4-AP (Fig. 5A), but the absorbance measured at 298 nm is the sum of absorbances from both 4-NP and 4-AP. Thus, the absorbance ratio method, which assumes that for a substance that obeys Beer Lambert's Law at all wavelengths, the ratio of absorbances at any two wavelengths is a constant value independent of concentration or pathlengths (Beckett and Stenlake, 1988), was used to determine the absorbance contribution of 4-NP at 298 nm using its absorbance at 400 nm (i.e. Abs_{298}) as a reference and by difference with the measured absorbance at 298 nm, the absorbance of 4-AP at 298 nm (i.e. Abs_{298}) was determined.

Rearranging Eqs. 2 and 3 leads to Eqs. 4 and 5, which were used to determine the rate constants, k_{NP}, and k_{AP}, based on 4-NP disappearance and 4-AP formation, respectively. The solver tool in MS Excel was used to fit the experimental data with Eqs. 4 and 5 using the least square method to determine k_{NP} and k_{AP}. The ratio $\varepsilon_{AP}/\varepsilon_{NP}$ was taken equal to 0.232 as determined from experimental data (Strachan et al., 2020).

$$C_{NPt}/C_{NP0} = \exp(-k_{NP}\cdot t) \quad (2)$$

$$C_{APt}/C_{NP0} = 1\text{-}\exp(-k_{AP}\cdot t) \quad (3)$$

$$Abs_{400\_t}/Abs_{400\_0} = \exp(-k_{NP}\cdot t) \quad (4)$$

$$Abs_{298\_t}/Abs_{400\_0} = (\varepsilon_{AP}/\varepsilon_{NP})[1\text{-}\exp(-k_{AP}\cdot t)] \quad (5)$$

Where: C_{NPt} and C_{NP0} are the concentrations of 4-NP at time t and time zero, respectively; C_{APt} is the concentrations of 4-AP at time t; Abs_{400_t} and Abs_{400_0} are the light absorbances at 400 nm at times t and zero, respectively; Abs_{298_t} is the determined light absorbance at 298 nm for 4-AP using the absorbance ratio method at time t; and k_{NP} and k_{AP} are the rate constants determined based on 4-NP disappearance and 4-AP appearance, respectively.

3. Results and discussion

3.1. Catalyst characterisation

3.1.1. FT-IR

FT-IR spectra of graphene nanoplatelets, MgAl-LDH and GNP/MgAl-LDH nanocomposite are reported in Fig. 1. On GNP sample, the characteristic peaks of graphene at 2990 cm^{-1} and 2880 cm^{-1} associated with asymmetric and symmetric vibration modes of groups (C–H) are observed (Ţucureanu et al., 2016). The peaks situated at 1060 cm^{-1} and 1380 cm^{-1} are assigned to the stretching vibrations of C–O and C–OH, respectively. Their appearance is due to GNP oxidation during its plasma oxygen treatment (Aravind et al., 2011; Song et al., 2015).

The FTIR spectrum of MgAl–LDH shows a typical peak of LDH represented by a strong peak at 3440 cm^{-1} which is attributed to the stretching of O−H groups associated with the interlayer water molecules and hydrogen bonding, and a weak peak at 1623 cm^{-1} due to OH bending of the interlayer water molecules. The strong peak at 1355 cm^{-1} is attributed to the vibration mode of CO_3^{2-} ions in the interlayer of MgAl-LDH while the weaker peak at 1100 cm^{-1} is attributed to interlayered SO_4^{2-} in the inorganic frame due to the asymmetric and symmetric stretching vibration of S═O (Duan et al., 2016; Mahjoubi et al., 2016). The bands in the range 500–800 cm^{-1} are attributable to M−O, O−M−O, and M−O−M lattice vibrations (M = Mg and Al) (Iqbal et al., 2020; Wen et al., 2013). Compared to MgAl–LDH and GNP separately, all their characteristic peaks are present in the spectrum of GNP/MgAl-LDH nanocomposite, which confirms the introduction of graphene nanoplatelets on MgAl-LDH.

3.1.2. XRD analysis

The XRD results are reported in Figs. 2A and 2B in the 10–70 2Θ and 5–70 2Θ ranges. Both GNP and AuNP/GNP showed two typical lines characteristic of graphene at 26.5° and 54.7° (Ren et al., 2020; Wang and Zhang, 2019). For all samples containing MgAl-LDH, the lines at 2Θ = 11.6° (003), 23.5° (006), 35.0° (012), 39.6° (015), 47.1° (018), 60.9° (110), and 62.3° (113) are characteristics of LDH phase as reported in other studies (Huang et al., 2018; Zhang et al., 2011). Additionally, a diffraction line at 26.5° corresponding to GNP phase confirms the intercalation of GNP in MgAl-LDH's structure. For AuNP/GNP/MgAl-LDH and AuNP/GNP, besides the diffraction lines

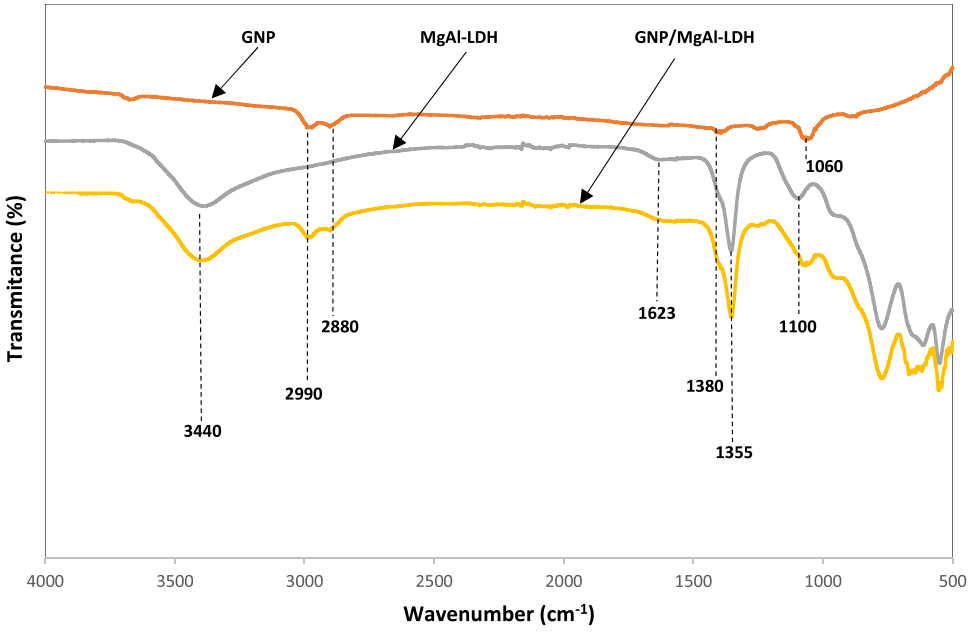

Fig. 1. FT-IR spectra of GNP, MgAl-LDH and GNP/MgAl-LDH nanocomposite.

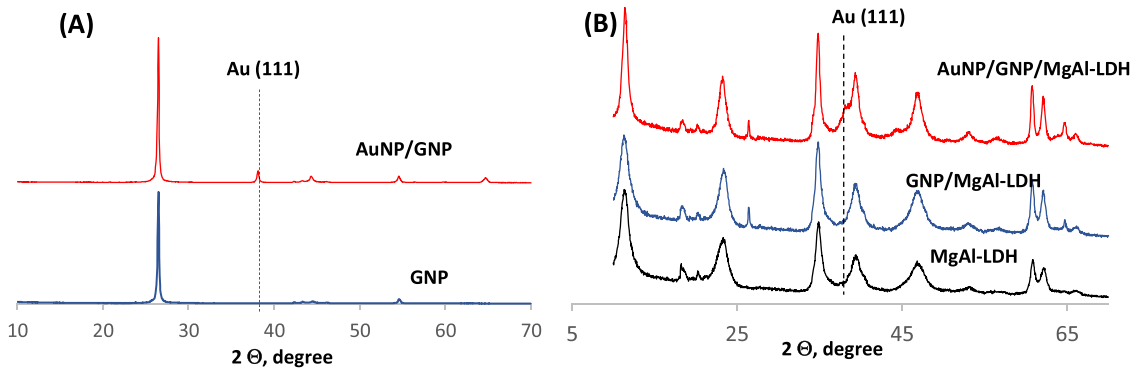

Fig. 2. XRD analysis (A) GNP and AuNP/GNP; (B) MgAl-LDH, GNP/MgAl-LDH, and AuNP/GNP/MgAl-LDH.

corresponding to MgAl-LDH and GNP/MgAl-LDH phases, diffraction lines corresponding to the gold phase are observed at $2\theta = 38.2°$, 44.5° and 64.7°, which can be assigned to the (111), (200), (220), indices, respectively, of metallic Au with a face centered cubic structure (JCPDS No. 04-0784). These results demonstrate the deposition of gold nanoparticles on GNP/MgAl-LDH nanocomposite.

3.1.3. TEM analysis

The extent of loading can be estimated by visual inspection of a series of Scanning Transmission Electron Microscopy (STEM) images under high-angle annular dark-field (HAADF) mode shown in Fig. 3. The HAADF-STEM images show platelet-like sheets on the samples containing MgAl-LDH and the winkled morphology of graphene in Fig. 3A while in Fig. 3C, GNP was mostly covered by MgAl-LDH structures. The dark field TEM micrographs confirmed the formation of approximately spherical AuNPs on the catalysts with particles being more homogeneously distributed over MgAl-LDH surface than on GNP surface (Fig. 3A,B). It can also be noted that the concentrations of AuNPs are much higher in catalysts containing MgAl-LDH (Fig. 3B,C). The AuNP/GNP/MgAl-LDH presents a broad particle size distribution with an average diameter of 11 nm (Fig. 3C), but the particle size histogram of AuNP/GNP (Fig. 3A) reveals a larger size distribution with particle sizes in the range 2 to ~30 nm with an average diameter of 14 nm. The narrowest particle size distribution was obtained for AuNP/MgAl-LDH with an average particle size of 4.7 nm. Other studies have also reported AuNP particle size distributions similar to the particle sizes reported in our study (Dou and Zhang, 2016; Panigrahi et al., 2007). Based on our results, a suggested scheme representing the structure of the AuNP/GNP/MgAl-LDH catalyst is simplified and presented in Fig. 3D.

3.1.4. Specific surface area and pore characteristics: BET/BJH analyses

The textural characteristics of the catalysts including pore volume, pore size distribution and specific surface area were analysed using nitrogen sorptometry measurements at 77 K. The nitrogen adsorption/desorption isotherms of the catalysts were similar (Fig. 4) and belonged to type IV of the IUPAC classification (ALOthman, 2012; Chen et al., 2017) with distinct H3-type hysteresis loops at high relative pressures, which is consistent with other studies on LDHs (Chen et al., 2017; Parida et al., 2012). This indicates that the MgAl-LDH catalysts have a mesoporous structure of slit-shaped pores due to aggregates of plate-like sheets (ALOthman, 2012), which is consistent with the TEM analysis. The average pore diameters were 10.4 nm and 8.4 nm for AuNP/GNP/MgAl-LDH and AuNP/MgAl-LDH catalysts, respectively, falling within the range of pore diameters of LDHs reported in the literature (Chen et al., 2017; Liu et al., 2019). Therefore, the intercalation of GNP within the structure of the MgAl-LDH increased its mesoporous diameter, by approximately 2 nm, which is consistent with the increased pore volume from 0.23 cm^3/g for AuNP/MgAl-LDH to 0.25 cm^3/g for AuNP/GNP/MgAl-LDH (Fig. 4 inset). This is also consistent with the slight reduction in the BET surface area of AuNP/GNP/MgAl-LDH (49 m^2/g) in comparison to AuNP/MgAl-LDH (51 m^2/g). The addition of GNP, which has lower surface area (Fig. 4 inset) and led to larger catalyst particle sizes (see TEM analysis), could also contributed to the slightly reduced surface area measured for AuNP/GNP/MgAl-LDH.

3.2. Catalytic activity for 4-nitrophenol reduction

To investigate the catalytic performance of the prepared samples, we selected the reduction of 4-NP by $NaBH_4$ to 4-AP at room temperature as a model reaction. The reaction was monitored by UV–Vis spectroscopy. Fig. 5A illustrates the characteristic UV–vis spectra of 4-NP solution with a maximum absorbance at 317 nm (Liu et al., 2017). However, in the presence of the reductant $NaBH_4$, the maximum absorbance shifts to 400 nm and the solution becomes yellow indicating the formation of 4-nitrophenolate ions ($4\text{-}NP^-$) because of the deprotonation of the hydroxyl group of 4-NP under the alkaline condition created by the addition of $NaBH_4$ (Liu et al., 2017). In the absence of the catalyst, there was no change in absorbance at 400 nm as function of time indicating that the reduction reaction does not occur in the presence of $NaBH_4$ only without the catalyst. However, by adding any of the three catalysts (AuNP/GNP/MgAl-LDH, AuNP/MgAl-LDH, or AuNP/GNP), the absorbance at 400 nm (i.e. 4-nitrophenolate) decreases rapidly with a concomitant increase in the maximum absorbance at 298 nm, indicting the formation of 4-aminophenol. Typical spectra measured at different times are shown for AuNP/GNP and AuNP/GNP/MgAl-LDH on Fig. 5(B, C). As can be seen, both catalysts are active in 4-nitrophenol reduction, with higher activity observed for AuNPs supported on GNP/MgAl-LDH nanocomposite; the catalytic reduction of 4-NP is complete within only 6 min over AuNP/GNP/MgAl-LDH but it took 15 min over AuNP/GNP.

The reaction rate constants, k_{NP}, and k_{AP} were then determined for the three catalysts AuNP/ MgAl-LDH, AuNP/GNP, and AuNP/GNP/MgAl-LDH. Fig. 5D shows the relationship between k_{AP} and k_{NP} obtained for the three catalysts and indicates that the rate constants determined for the disappearance of 4-NP and the appearance of 4-AP agree very well (within 5 % error). This indicates proportional transformation of 4-NP to 4-AP and the reaction is near stoichiometric with insignificant loss of 4-NP or 4-AP to other products. This was further corroborated by calculating the ratio of the molar concentration of 4-AP at the end of the reaction to that of 4-NP at time zero and a ratio close to 1.0 (>0.90) was obtained for the experiments conducted. Since both k_{AP} and k_{NP} were not significantly different, the rate constant of the reaction, k_{app}, was taken as the average of k_{AP} and k_{NP}. The calculated rate constants, k_{app}, for the three catalysts are shown on Fig. 5E. The figure shows that AuNP on GNP/MgAl-LDH gave the highest rate constant followed by MgAl-LDH and GNP. The results indicate that MgAl-LDH support has increased the reaction rate by approximately 2.5 times as compared to GNP support on its own, and GNP has increased the reaction rate by approximately 1.5 times as compared to MgAl-LDH support on its own.

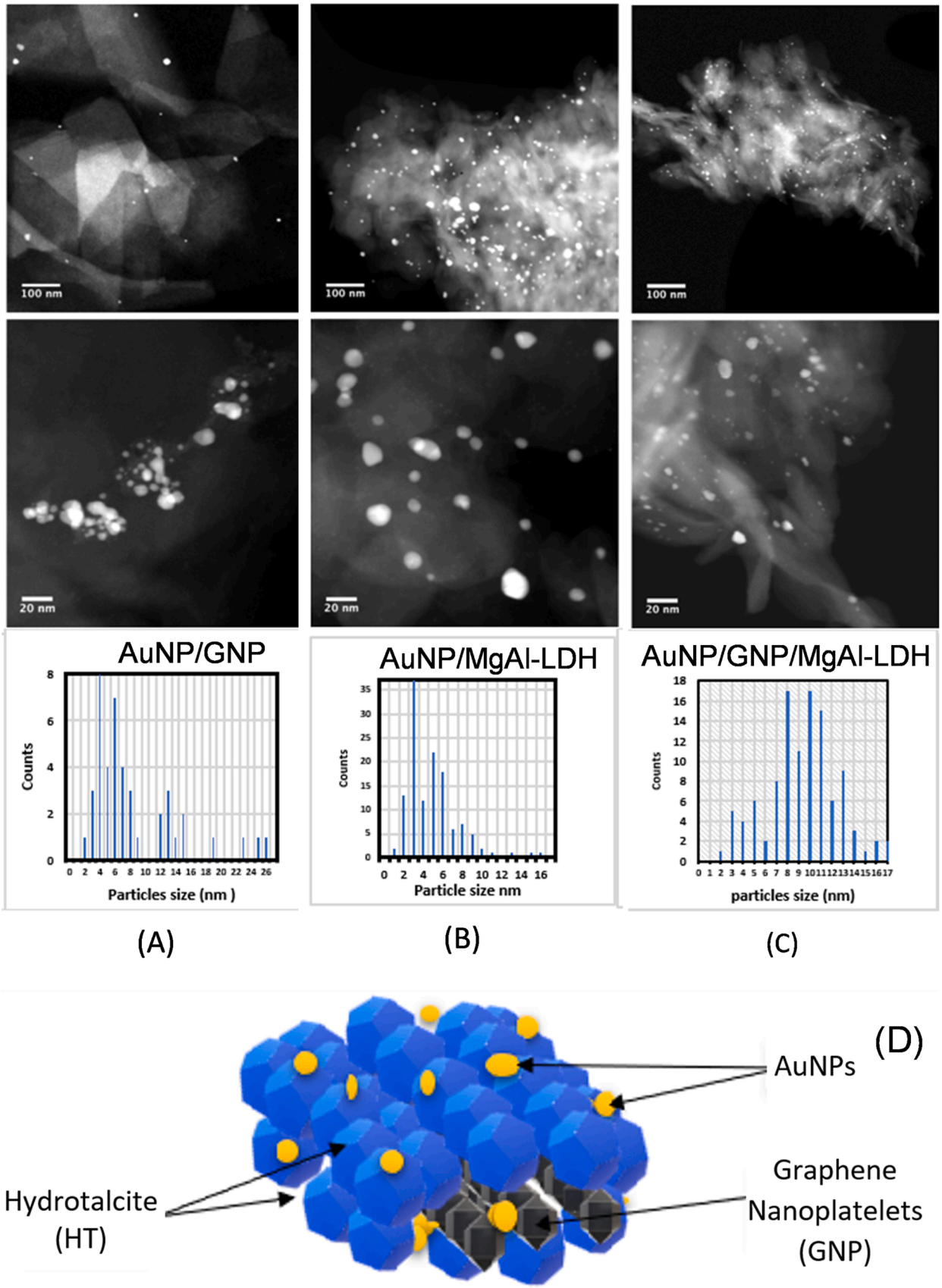

Fig. 3. Dark field STEM micrographs, TEM images and particle size distributions of (A) AuNP/GNP, (B) AuNP/MgAl-LDH, (C) AuNP/GNP/MgAl-LDH, and (D) schematic representation of the AuNP/GNP/MgAl-LDH catalyst.

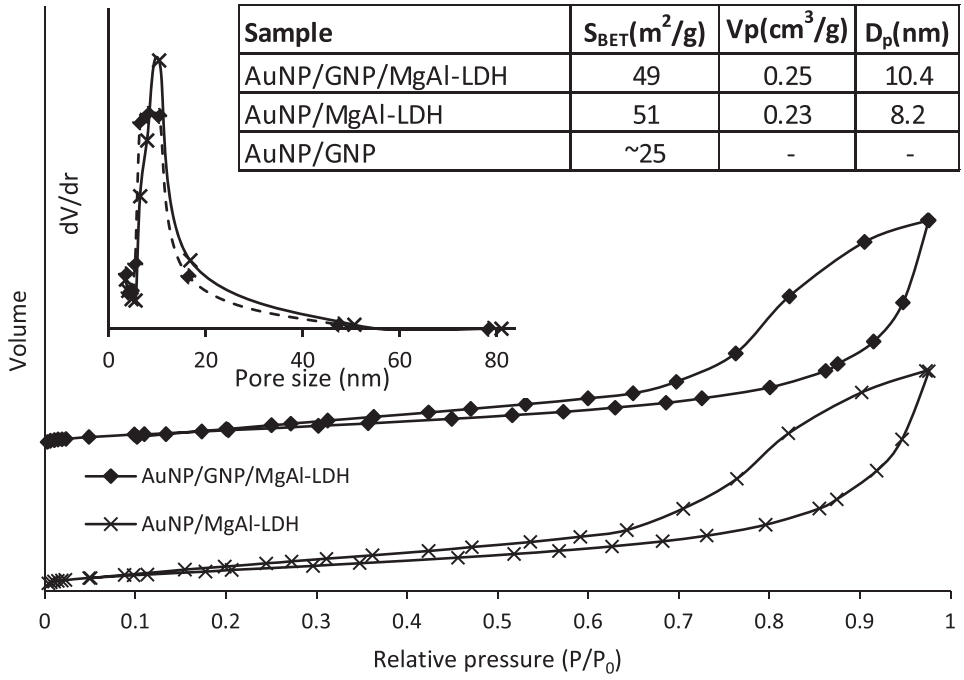

Fig. 4. Nitrogen adsorption/desorption isotherms at 77 K and corresponding pore size distributions, average pore sizes, pore volumes, and specific BET surface areas (insets) for AuNP/GNP/MgAl-LDH and AuNP/MgAl-LDH catalysts.

Zeta potential measurements have shown that hydrotalcite-containing materials have positively charged surfaces even in the presence of graphene oxide, characterised by a strong negatively charged surface, (Dou and Zhang, 2016; Liu et al., 2019; Nguyen et al., 2019). Therefore, the enhanced reaction rate constants by AuNP/GNP/MgAl-LDH could be explained by a higher attraction of the reactant anions 4-NP$^-$ and BH_4 to the positively charged MgAl-LDH surface (Nguyen et al., 2019), thereby lowering the kinetic barrier and enhancing the catalytic activity of the catalyst towards the reduction reaction. In contrast, graphene nanoplatelets are characterised by negative surface charge (Kazi et al., 2015), thus they limit the attraction of the reactants to the catalyst. In addition, as observed in the TEM analysis, AuNP/GNP catalyst had a higher average AuNPs particle size and a lower concentration of AuNPs than AuNP/GNP/MgAl-LDH, which further supports the higher catalytic activity of AuNP/GNP/MgAl-LDH since smaller particles are more active in comparison to larger particles and higher concentration means higher active catalytic sites. This is at the expense of a slightly higher BET surface area for AuNP/MgAl-LDH (Fig. 4 inset), though. Comparing the catalytic activity of AuNP/GNP/MgAl-LDH prepared in this study, our catalyst presented higher catalytic activity than that reported in other studies who used catalysts based on gold nanoparticles supported on graphene. For example, a rate constant of 1.96 10^{-3} s^{-1} (0.118 min^{-1}) was obtained using Au-NPs/rGo microspheres and a molar ratio of $NaBH_4$ to 4-NP of 20 (Li et al., 2019), and 2.06 10^{-3} s^{-1} (0.124 min^{-1}) was obtained over hybrid Au-GO nanocomposites using a molar ratio of $NaBH_4$ to 4-NP of 50 (Choi et al., 2011) giving lower catalytic activities than our catalyst by the factors 5.5 and 5.3, respectively. In addition, we calculated the ratio of the rate constant to the AuNP content (in L/(s.g Au)) and found that this study's catalyst gave reaction rate constants about 20 times higher than those reported by (Choi et al., 2011; Li et al., 2019).

3.3. Catalytic mechanism

As discussed in the previous section, AuNP/GNP/MgAl-LDH plays a key role in enhancing the reduction of nitrophenol reaction. This enhancement could be attributed to increased adsorption of 4-NP reactants on the positively charged MgAl-LDH surface (Gao et al., 2022) and enhanced electron transfer by GNP (Fig. 6 A). 4-NP has a pKa value of 7.15, which implies that at a neutral pH, about 41 % of its original concentration is found dissociated into 4-nitrophenolate anion and as pH increases above neutral pH, the anion concentration increases (Fig. 6B). This enhanced attraction of the 4-NP anion to the surface of the catalyst is accompanied by the adsorption of the borohydride ions onto the surface of gold nanoparticles transferring its electrons to AuNP, which are further carried through the highly electrophile graphene layers to end up at the interface of the catalyst (Fig. 6 A). The surplus of electrons added to the surface of the catalyst allows the uptake of electrons by 4-NP adsorbed on the surface of the catalyst. This leads to the reduction of 4-NP to 4-AP followed by detachment of the product 4-AP leaving the catalytic site free for a new catalytic cycle to start again.

3.4. Catalyst reuse

We have also tested the stability of AuNP/GNP/MgAl-LDH catalysts after reuse over five successive reaction cycles. In a typical experiment, the collected mass of catalyst by filtration and washing with DI water was then redispersed in a mixture of 4-NP and $NaBH_4$ and reused to evaluate its catalytic activity. The results of 4-NP reaction conversion over 6 min reaction time in each cycle were used to calculate the rate constant, k_{appi}, obtained in each cycle, *i*. The values of k_{appi} were scaled to the mass of catalyst used in cycle *i* and the ratio of scaled k_{appi} at each cycle to the first cycle, r_k, is reported in Fig. 7. As can be observed in Fig. 7, for the first three cycles, r_k remained unchanged, but after the third cycle, a slight decrease in activity was observed (r_k~0.97). This indicates that the catalyst retained high catalytic activity indicating its excellent reusability, which is in agreement with other studies (Cho et al., 2018; Dou and Zhang, 2016). The slight reduction in catalyst efficiency after three cycles could be due to accumulation of near-surface ions concentration (Goyal and Koper, 2021) or even chemisorption of impurities as a result of repeated use (Satyanarayana et al., 2016), which reduces the number of available catalytic sites for the adsorption of reactants between cycles; adsorption is an important step in the

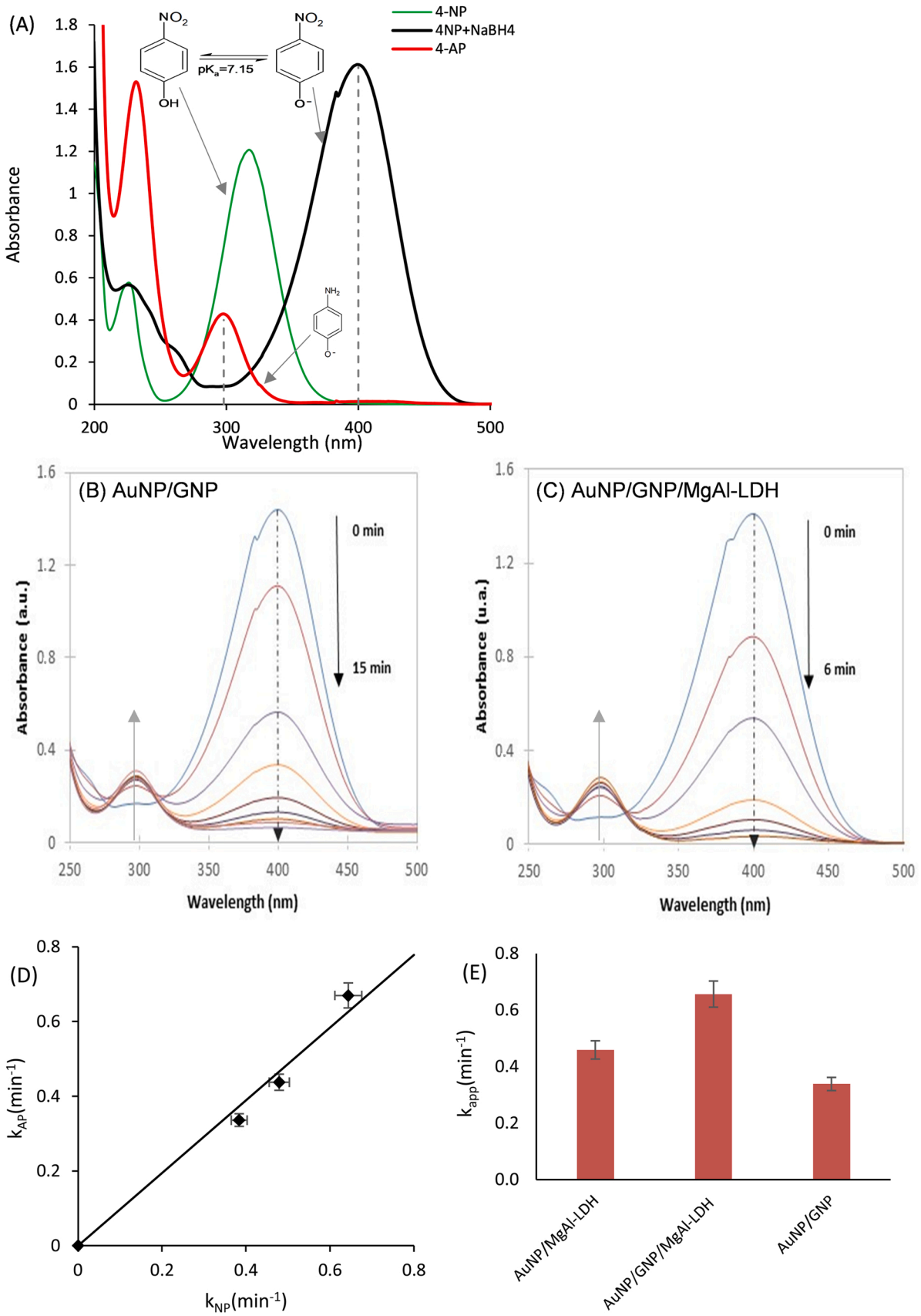

Fig. 5. UV–Vis absorption spectra of: (A) 4-NP, 4-NP with $NaBH_4$, and 4-AP; (B) 4-NP reduction by $NaBH_4$ over AuNP/GNP, (C) 4-NP reduction by $NaBH_4$ over AuNP/GNP/MgAl-LDH. (D) relationship between k_{AP} and k_{NP}, and (E) rate constants for the different catalysts AuNP/MgAl-LDH, AuNP/GNP/MgAl-LDH, and AuNP/GNP.

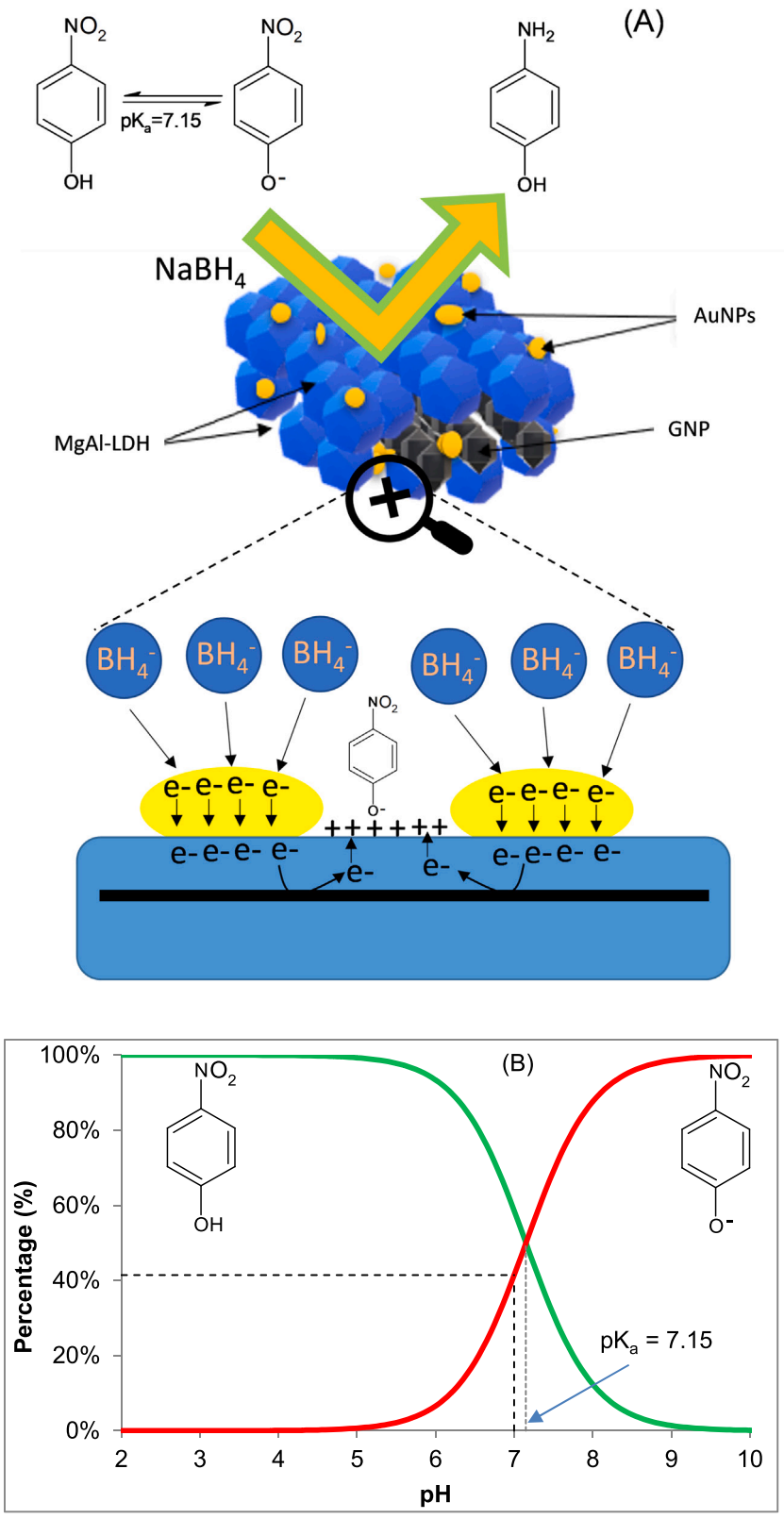

Fig. 6. (A) Suggested scheme for AuNP/GNP/MgAl-LDH catalyst and its mechanism for the reduction of nitrophenol in the presence of $NaBH_4$.; (B) Calculated nitrophenol speciation (pKa=7.15).

reduction mechanism as discussed above. In the presence of a strong reducing agent $NaBH_4$, it is also possible that during recycling of the catalyst, slight damage to the LDH plates takes place (Dou and Zhang, 2016). Although, these phenomena are reported in the literature as possible reasons for observed catalytic reduction during catalyst reuse, the impact on our hybrid catalyst appears being minimum.

Therefore, this study clearly demonstrates the crucial role that the support material plays for enhancing the catalytic activity of gold

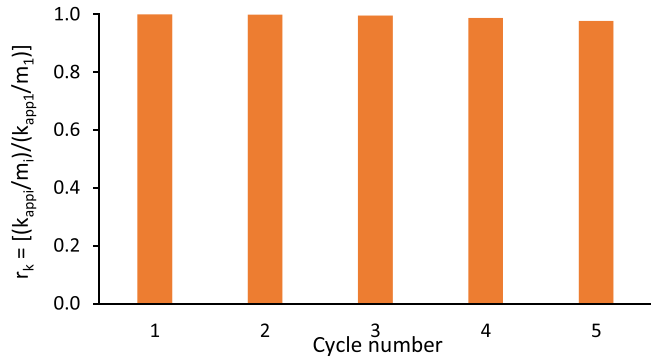

Fig. 7. Conversion of 4-NP at different cycles (k_{app1} and k_{appi} are the rate constants at cycles 1 and i, respectively, and m_1 and m_i are the catalyst masses at cycles 1 and i, respectively).

nanoparticles in the reduction of 4-nitrophenol to 4-aminophenol reaction. This study contributes to emphasising that gold is not a poor candidate catalyst, though it is considered as an unreactive noble metal, and adds to the literature supporting this (Sankar et al., 2020). In recent years, academic interest on the application of LDHs in catalysis has grown exponentially (Zhao et al., 2020), thus this study adds to this field where selection and design of novel support structures for catalysts is currently an active research area (Sankar et al., 2020; Zhao et al., 2020). The intercalation of GNP in the support structure has enhanced the catalytic activity of the catalyst. In a study by Guo et al. (Guo et al., 2020), it was also shown that the decoration of MgAl-LDH by carbon material improved the catalytic activity of the gold catalyst towards benzyl alcohol conversion as well as enhanced the structural stability of the catalyst due to strong interactions between Au and the surface of the support material. Our results suggest that MgAl-LDH enhances the adsorption of the reactants while GNP enhances electron transfer, thus promoting the reduction of 4-NP through a cooperative effect of well dispersed AuNPs and surface positive charges as demonstrated in Fig. 6. Moreover, the successful use of AuNP/GNP/MgAl-LDH as a catalyst and given its facile synthesis may offer a new route for the exploitation of AuNPs at commercial level while opening a promising approach to develop highly efficient AuNPs-based catalysts for various heterogenous catalytic reactions.

4. Conclusions

A novel catalyst based on gold nanoparticles (AuNPs) supported on GNP/MgAl-LDH nanocomposites (AuNP/GNP/MgAl-LDH) was synthesised by the deposition-precipitation method and compared to AuNPs supported on GNP (AuNP/GNP) and on MgAl-LDH (AuNP/MgAl-LDH). This novel catalyst exhibited high catalytic activity in 4-nitrophenol reduction to 4-aminophenol with equivalent reaction rate constants for the disappearance of 4-NP and appearance of 4-AP. The reaction rate constants indicated that AuNP/GNP/MgAl-LDH had the highest activity followed by AuNP/MgAl-LDH and AuNP/GNP. Using GNP as support for AuNPs lead to the formation of particles with larger size and lower concentration than the GNP/MgAl-LDH support. Through STEM analysis, MgAl-LDH was found to provide uniform binding sites for AuNPs, which effectively prevented the agglomeration of AuNPs and enhanced the catalytic activity. The positive charge imparted by MgAl-LDH, which would attract the negatively charged reactants (4-NP^- and BH_4^-), was also postulated as a reason for the observed enhanced catalytic activity of AuNP/GNP/MgAl-LDH catalyst. Furthermore, AuNP/GNP/MgAl-LDH exhibited a good stability and was reusable in consecutive cycles without losing significant catalytic activity.

Declaration of Competing Interest

The authors declare that they have no known competing financial interests or personal relationships that could have appeared to influence the work reported in this paper.

Acknowledgement

Meriem Banou acknowledges the financial support from the Ministry of Higher Education of Algeria under the National Exceptional Program Grant (PNE). The authors acknowledge access to the Swansea University Advanced Imaging of Materials (AIM) Facility for catalyst characterisation. AIM is funded in part by the EPSRC (EP/M028267/1), the European Regional Development Fund through the Welsh Government (80708) and the Welsh Government's Ser Cymru Program.

References

Alawi, O.A., Sidik, N.A.C., Kazi, S.N., Najafi, G., 2019. Graphene nanoplatelets and few-layer graphene studies in thermo-physical properties and particle characterization. J. Therm. Anal. Calorim. 135, 1081–1093.
ALOthman, Z.A., 2012. A review: fundamental aspects of silicate mesoporous materials. Materials 5, 2874–2902.
Alshammari, K., Niu, Y., Palmer, R.E., Dimitratos, N., 2020. Optimization of sol-immobilized bimetallic Au–Pd/TiO2 catalysts: reduction of 4-nitrophenol to 4-aminophenol for wastewater remediation. Philos. Trans. R. Soc. A Math., Phys. Eng. Sci. 378, 20200057.
Aravind, S.S.J., Baby, T.T., Arockiadoss, T., Rakhi, R.B., Ramaprabhu, S., 2011. A cholesterol biosensor based on gold nanoparticles decorated functionalized graphene nanoplatelets. Thin Solid Films 519, 5667–5672.
Asiabi, H., Yamini, Y., Shamsayei, M., Tahmasebi, E., 2017. Highly selective and efficient removal and extraction of heavy metals by layered double hydroxides intercalated with the diphenylamine-4-sulfonate: a comparative study. Chem. Eng. J. 323, 212–223.
Beckett, A.H., Stenlake, J.B., 1988. Practical Pharmaceutical Chemistry: Part II, The Athlone Press, London.
Beltrán, F.J., Álvarez, P.M., Gimeno, O., 2019. Graphene-based catalysts for ozone processes to decontaminate water. Molecules 24, 3438.
Bleach, R., Karagoz, B., Prakash, S.M., Davis, T.P., Boyer, C., 2014. In situ formation of polymer–gold composite nanoparticles with tunable morphologies. ACS Macro Lett. 3, 591–596.
Cataldi, P., Athanassiou, A., Bayer, I.S., 2018. Graphene nanoplatelets-based advanced materials and recent progress in sustainable applications. Appl. Sci. 8, 1438.
Cavani, F., Trifirò, F., Vaccari, A., 1991. Hydrotalcite-type anionic clays: preparation, properties and applications. Catal. Today 11, 173–301.
Chegel, V., Rachkov, O., Lopatynskyi, A., Ishihara, S., Yanchuk, I., Nemoto, Y., Hill, J.P., Ariga, K., 2012. Gold nanoparticles aggregation: drastic effect of cooperative functionalities in a single molecular conjugate. J. Phys. Chem. C 116, 2683–2690.
Chen, C.-R., Zeng, H.-Y., Xu, S., Liu, X.-J., Duan, H.-Z., Han, J., 2017. Preparation of mesoporous material from hydrotalcite/carbon composite precursor for chromium (VI) removal. J. Taiwan Inst. Chem. Eng. 70, 302–310.
Chen, S., Xiang, Y., Peng, C., Xu, W., Banks, M.K., Wu, R., 2019. Synthesis of a novel graphene-based gold nanocomposite using PVEIM-b-PNIPAM as a stabilizer and its thermosensitivity for the catalytic reduction of 4-nitrophenol. Inorg. Chem. Front. 6, 903–913.
Cho, H.R., Kwon, Y.M., Lee, Y.J., Park, Y.A., Ji, H.G., Lee, J.H., 2018. Morphological control of gold nanoparticles on exfoliated layers of layered double hydroxide: a reusable hybrid catalyst for the reduction of p-nitrophenol. Appl. Clay Sci. 156, 187–194.
Choi, Y., Bae, H.S., Seo, E., Jang, S., Park, K.H., Kim, B.-S., 2011. Hybrid gold nanoparticle-reduced graphene oxide nanosheets as active catalysts for highly efficient reduction of nitroarenes. J. Mater. Chem. 21, 15431–15436.
Dou, L., Zhang, H., 2016. Facile assembly of nanosheet array-like CuMgAl-layered double hydroxide/rGO nanohybrids for highly efficient reduction of 4-nitrophenol. J. Mater. Chem. A 4, 18990–19002.
Duan, H.-Z., Zeng, H.-Y., Xiao, H.-M., Chen, C.-R., Xiao, G.-F., Zhao, Q., 2016. Optimization of ammonia nitrogen removal by SO42− intercalated hydrotalcite using response surface methodology. RSC Adv. 6, 48329–48335.
Gao, F., Xu, X.R., Yang, J.Y., 2022. Removal of p-nitrophenol from simulated sewage using MgCo-3D hydrotalcite nanospheres: capability and mechanism. RSC Adv. 12, 27044–27054.
Gemini, V.L., Gallego, A., de Oliveira, V.M., Gomez, C.E., Manfio, G.P., Korol, S.E., 2005. Biodegradation and detoxification of p-nitrophenol by Rhodococcus wratislaviensis. Int. Biodeterior. Biodegrad. 55, 103–108.
Goyal, A., Koper, M.T.M., 2021. The interrelated effect of cations and electrolyte pH on the hydrogen evolution reaction on gold electrodes in alkaline media. Angew. Chem. Int. Ed. 60, 13452–13462.
Guo, Y.J., Fan, L.P., Liu, M.R., Yang, L., Fan, G.L., Li, F., 2020. Nitrogen-doped carbon quantum dots-decorated Mg-Al layered double hydroxide-supported gold nanocatalysts for efficient base-free oxidation of benzyl alcohol. Ind. Eng. Chem. Res. 59, 636–646.

Hao, S., Li, S., Jia, Z., 2020. Tunable synthesis of Pd/COF-LZU1 for efficient catalysis in nitrophenol reduction. J. Nanopart. Res. 22, 270.
Haruta, M., Yamada, N., Kobayashi, T., Iijima, S., 1989. Gold catalysts prepared by coprecipitation for low-temperature oxidation of hydrogen and of carbon monoxide. J. Catal. 115, 301–309.
Hashimi, A.S., Nohan, M.A.N.M., Chin, S.X., Zakaria, S., Chia, C.H., 2019. Rapid catalytic reduction of 4-nitrophenol and clock reaction of Methylene Blue using copper nanowires. Nanomaterials 9, 936.
Huang, Q., Chen, Y., Yu, H., Yan, L., Zhang, J., Wang, B., Du, B., Xing, L., 2018. Magnetic graphene oxide/MgAl-layered double hydroxide nanocomposite: one-pot solvothermal synthesis, adsorption performance and mechanisms for Pb2+, Cd2+, and Cu2+. Chem. Eng. J. 341, 1–9.
Iben Ayad, A., Luart, D., Ould Dris, A., Guénin, E., 2020. Kinetic analysis of 4-nitrophenol reduction by "Water-Soluble" palladium nanoparticles. Nanomaterials 10, 1169.
Iqbal, M.A., Secchi, M., Iqbal, M.A., Montagna, M., Zanella, C., Fedel, M., 2020. MgAl-LDH/graphene protective film: insight into LDH-graphene interaction. Surf. Coat. Technol. 401, 126253.
Jordi, R.G., Young, B.D., Bryson, A.W., 1991. Gold adsorption on activated carbon and the effect of suspended solids and dissolved silicon dioxide. Chem. Eng. Commun. 102, 127–147.
Kazi, S.N., Badarudin, A., Zubir, M.N.M., Ming, H.N., Misran, M., Sadeghinezhad, E., Mehrali, M., Syuhada, N.I., 2015. Investigation on the use of graphene oxide as novel surfactant to stabilize weakly charged graphene nanoplatelets. Nanoscale Res. Lett. 10, 15.
Kuge, Ki, Calzaferri, G., 2003. Gold-loaded zeolite A. Microporous Mesoporous Mater. 66, 15–20.
Li, M., Chen, G., 2013. Revisiting catalytic model reaction p-nitrophenol/NaBH4 using metallic nanoparticles coated on polymeric spheres. Nanoscale 5, 11919–11927.
Li, N., Zhang, F., Wang, H., Hou, S., 2019. Catalytic degradation of 4-nitrophenol in polluted water by three-dimensional gold nanoparticles/reduced graphene oxide microspheres. Eng. Sci. 7, 72–79.
Liu, C., Zhang, M., Pan, G., Lundehøj, L., Nielsen, U.G., Shi, Y., Hansen, H.C.B., 2019. Phosphate capture by ultrathin MgAl layered double hydroxide nanoparticles. Appl. Clay Sci. 177, 82–90.
Liu, S., Qileng, A., Huang, J., Gao, Q., Liu, Y., 2017. Polydopamine as a bridge to decorate monodisperse gold nanoparticles on Fe3O4 nanoclusters for the catalytic reduction of 4-nitrophenol. RSC Adv. 7, 45545–45551.
Ma, T., Yang, W., Liu, S., Zhang, H., Liang, F., 2017. A comparison reduction of 4-nitrophenol by gold nanospheres and gold nanostars. Catalysts 7, 38.
Mahjoubi, F.Z., Khalidi, A., Abdennouri, M., Barka, N., 2016. M-Al-SO4 layered double hydroxides (M=Zn, Mg or Ni): synthesis, characterization and textile dyes removal efficiency. Desalin. Water Treat. 57, 21564–21576.
Marinoiu, A., Raceanu, M., Andrulevicius, M., Tamuleviciene, A., Tamulevicius, T., Nica, S., Bala, D., Varlam, M., 2020. Low-cost preparation method of well dispersed gold nanoparticles on reduced graphene oxide and electrocatalytic stability in PEM fuel cell. Arab. J. Chem. 13, 3585–3600.
Nguyen, T.D., Tran, B.A., Vu, K.O., Nguyen, A.S., Trinh, A.T., Pham, G.V., To, T.X.H., Phan, M.V., Phan, T.T., 2019. Corrosion protection of carbon steel using hydrotalcite/graphene oxide nanohybrid. J. Coat. Technol. Res. 16, 585–595.
Novoselov, K.S., Geim, A.K., Morozov, S.V., Jiang, D., Katsnelson, M.I., Grigorieva, I.V., Dubonos, S.V., Firsov, A.A., 2005. Two-dimensional gas of massless Dirac fermions in graphene. Nature 438, 197–200.
Novoselov, K.S., Geim, A.K., Morozov, S.V., Jiang, D., Zhang, Y., Dubonos, S.V., Grigorieva, I.V., Firsov, A.A., 2004. Electric field effect in atomically thin carbon films. Science 306, 666–669.
Panigrahi, S., Basu, S., Praharaj, S., Pande, S., Jana, S., Pal, A., Ghosh, S.K., Pal, T., 2007. Synthesis and size-selective catalysis by supported gold nanoparticles: study on heterogeneous and homogeneous catalytic process. J. Phys. Chem. C 111, 4596–4605.
Parida, K., Mohapatra, L., Baliarsingh, N., 2012. Effect of Co2+ substitution in the framework of carbonate intercalated Cu/Cr LDH on structural, electronic, optical, and photocatalytic properties. J. Phys. Chem. C 116, 22417–22424.
Plant, S.R., Cao, L., Yin, F., Wang, Z.W., Palmer, R.E., 2014. Size-dependent propagation of Au nanoclusters through few-layer graphene. Nanoscale 6, 1258–1263.
Qiu, L., Peng, Y., Liu, B., Lin, B., Peng, Y., Malik, M.J., Yan, F., 2012. Polypyrrole nanotube-supported gold nanoparticles: an efficient electrocatalyst for oxygen reduction and catalytic reduction of 4-nitrophenol. Appl. Catal. A Gen. 413–414, 230–237.
Ren, Y., Rao, R., Bhusal, S., Varshney, V., Kedziora, G., Wheeler, R., Kang, Y., Roy, A., Nepal, D., 2020. Hierarchical assembly of gold nanoparticles on graphene nanoplatelets by spontaneous reduction: implications for smart composites and biosensing. ACS Appl. Nano Mater. 3, 8753–8762.
Richardson, I.G., 2013. Zn- and Co-based layered double hydroxides: prediction of the a parameter from the fraction of trivalent cations and vice versa. Acta Crystallogr B Struct. Sci. Cryst. Eng. Mater. 69, 414–417.
Sankar, M., He, Q., Engel, R.V., Sainna, M.A., Logsdail, A.J., Roldan, A., Willock, D.J., Agarwal, N., Kiely, C.J., Hutchings, G.J., 2020. Role of the support in gold-containing nanoparticles as heterogeneous catalysts. Chem. Rev. 120, 3890–3938.
Satyanarayana, C.V., Srikant, D., Gurav, H.R., 2016. Chapter 5 - catalyst deactivation and regeneration. In: Joshi, S.S., Ranade, V.V. (Eds.), Industrial Catalytic Processes for Fine and Specialty Chemicals. Elsevier, Amsterdam, pp. 187–219.
Song, Y., Yu, J., Yu, L., Alam, F.E., Dai, W., Li, C., Jiang, N., 2015. Enhancing the thermal, electrical, and mechanical properties of silicone rubber by addition of graphene nanoplatelets. Mater. Des. 88, 950–957.
Strachan, J., Barnett, C., Masters, A.F., Maschmeyer, T., 2020. 4-Nitrophenol reduction: probing the putative mechanism of the model reaction. ACS Catal. 10, 5516–5521.
Ţucureanu, V., Matei, A., Avram, A.M., 2016. FTIR spectroscopy for carbon family study. Crit. Rev. Anal. Chem. 46, 502–520.
Verma, A.D., Mandal, R.K., Sinha, I., 2015. Kinetics of p-Nitrophenol reduction catalyzed by PVP stabilized copper nanoparticles. Catal. Lett. 145, 1885–1892.
Wang, X., Zhang, L., 2019. Green and facile production of high-quality graphene from graphite by the combination of hydroxyl radicals and electrical exfoliation in different electrolyte systems. RSC Adv. 9, 3693–3703.
Wen, T., Wu, X., Tan, X., Wang, X., Xu, A., 2013. One-pot synthesis of water-swellable Mg–Al layered double hydroxides and graphene oxide nanocomposites for efficient removal of As(V) from aqueous solutions. ACS Appl. Mater. Interfaces 5, 3304–3311.
Yam, K.M., Guo, N., Jiang, Z., Li, S., Zhang, C., 2020. Graphene-based heterogeneous catalysis: role of graphene. Catalysts 10, 53.
Yuzawa, H., Yoshida, T., Yoshida, H., 2012. Gold nanoparticles on titanium oxide effective for photocatalytic hydrogen formation under visible light. Appl. Catal. B Environ. 115–116, 294–302.
Zhang, F., Zhao, X., Feng, C., Li, B., Chen, T., Lu, W., Lei, X., Xu, S., 2011. Crystal-face-selective supporting of gold nanoparticles on layered double hydroxide as efficient catalyst for epoxidation of styrene. ACS Catal. 1, 232–237.
Zhang, Q., Fan, X., Wang, H., Chen, S., Quan, X., 2016. Fabrication of Au/CNT hollow fiber membrane for 4-nitrophenol reduction. RSC Adv. 6, 41114–41121.
Zhao, G.Q., Zou, J., Chen, X.Q., Yu, J.G., Jiao, F.P., 2020. Layered double hydroxides materials for photo(electro-) catalytic applications. Chem. Eng. J. 397, 31.
Zhu, L., Letaief, S., Liu, Y., Gervais, F., Detellier, C., 2009. Clay mineral-supported gold nanoparticles. Appl. Clay Sci. 43, 439–446.